

**GT2011-46466**

## **Modeling of Inlet Distortion using a Combined Turbofan and Nacelle Inlet Model during Crosswind and Low Speed Forward Operation**

**Kiran Vunnam and Robert Hoover**

Honeywell Aerospace  
Phoenix, Arizona USA

### **ABSTRACT**

Inlet distortion on turbofan nacelles during crosswind and low speed forward operation is an area of concern in the gas turbine engine community. Specifically for aft fuselage mounted nacelles, flow into the inlet is affected by the turning of the airflow at the inlet for crosswind operation, and by fuselage interference effects, such as fuselage based vortices, during low-speed forward operation.

A common process of modeling airflow through a turbofan inlet in crosswind and low-speed forward operation is to model the flow boundary, at the fan leading edge location, as a static pressure boundary. For this process, the fan face is represented by a two-dimensional static pressure profile as a function of radius. This process assumes the static pressure at the fan face is uniform circumferentially. In conditions where non-axisymmetric flow effects are present at the fan boundary, such as flow separation in the inlet or local fuselage based ground vortices, an axisymmetric pressure boundary at the fan face is inappropriate. The ingestion of a fuselage based ground vortex will also impact the prediction of inlet distortion into a turbofan inlet.

An improved methodology is to model the complete fan and fan stator system using a frozen rotor in a rotating reference frame. This allows the three dimensional flow effects of the fan and stator system to be better modeled within the CFD analysis by allowing the physical geometry of the modeled fan to set the flow characteristics circumferentially in the inlet.

The CFD analyses were performed using two methods: (1) with airflow through the nacelle driven by a static pressure boundary at the fan face, and (2) with the fan system modeled as a frozen rotor in a rotating reference frame. The CFD results were evaluated using ARP 1419 circumferential and radial distortion descriptors (Reference 1) at the nacelle's aerodynamic interface plane location. Results from the fan system CFD analyses are compared to typical values from distortion testing and to CFD results using a static pressure

profile boundary condition at the fan face.

The goal of this evaluation is to combine the aircraft nacelle and the fan rotor and stator in order to model the impact of a fuselage vortex on inlet distortion where flow through the inlet is set by the fan geometry and fan speed.

Initial studies on the isolated nacelle have predicted the effects of ground based vortices on the fan flow at various crosswind velocities. In the current study the effects of fuselage and ground based vortices are studied at various crosswind and head wind velocities at ground idle and takeoff operating conditions.

### **INTRODUCTION**

Pressure distortion within turbofan nacelle inlets during crosswind and low speed forward operation is an area of concern in the gas turbine engine community. The current accepted certification process for the evaluation of inlet distortion is by test. However, improvements in commercial CFD codes and computing systems allow the opportunity to model nacelle inlet distortion levels and trends prior to test.

Inlet distortion is generally at the highest levels during crosswind and low-speed forward operation. Understanding the flow structure and resulting pressure distortion is critical to optimizing the fuselage/pylon/nacelle system and can minimize testing required for aircraft certification.

Accurately modeling distortion caused by crosswind and forward velocity operation with contributing fuselage based vortices using the commercially available software is the challenge. The analysis becomes much more detailed when the CFD model includes the fan rotor and stator system along with the aircraft nacelle.

The impact of ground vortices has been documented since the advent of turbojet and turbofan engine designs (Reference 2). The placement of high volumetric flow rate, high velocity inlets near the ground for under wing engine installations

caused issues with foreign object ingestion into the engine and operability issues for the engine fan and compressor. These effects were attributed to ground vortices (Reference 3, Reference 4). Ground vortex formation in crosswind and low forward speed operation was studied discussed in previous journal articles (Reference 5, Reference 6).

Numerical modeling of ground vortices and their ingestion into an underwing nacelle installation was documented by Murphy and MacManus (Reference 7). Vortex formation to fuselage and wing surfaces on aft mounted fuselage nacelle installations is discussed in SAE AIR5686 (Reference 8).

This paper presents qualitative results from CFD analyses of vortices emanating from the fuselage surface for a fuselage mounted nacelle, as opposed to vortices emanating from the ground surface for an underwing mounted nacelle. The paper also provides quantitative results for circumferential and radial distortion for a typical fuselage mounted nacelle business jet application.

Previously, a CFD evaluation of the HTF7000 inlet was conducted without the fan rotor and stator system modeled. In lieu of the HTF7000 fan stator rotor system, a static pressure profile at the fan face location was supplied for a takeoff power-set by the HTF7000 fan aerodynamics group at Honeywell. The fan profile plotted as local static pressure normalized by freestream total pressure is shown in Figure 1.

Aerodynamic modeling issues arise in using static pressure profiles for models where flow recirculation may occur at the flow exit boundary. In high velocity crosswind conditions, flow separation off the upwind portion of the inlet lip can occur. This flow separation may not re-attach to the inlet diffuser surface and flow recirculation will occur at the inlet fan face flow boundary. This is not a realistic flow condition for the inlet and fan rotor systems. For a stable (non-surge) inlet and fan rotor system airflow will not backflow from the fan leading edge. To better model in CFD the inlet fan rotor system, the effects of the full inlet-fan rotor-stator system needs to be modeled.

To model this effect, the full HTF7000 22 blade fan rotor and associated stator system was added to the base aircraft and nacelle model geometry. The CFD model was created as a frozen rotor in a rotating reference frame with interfaces on either side, axially, of the fan rotor.

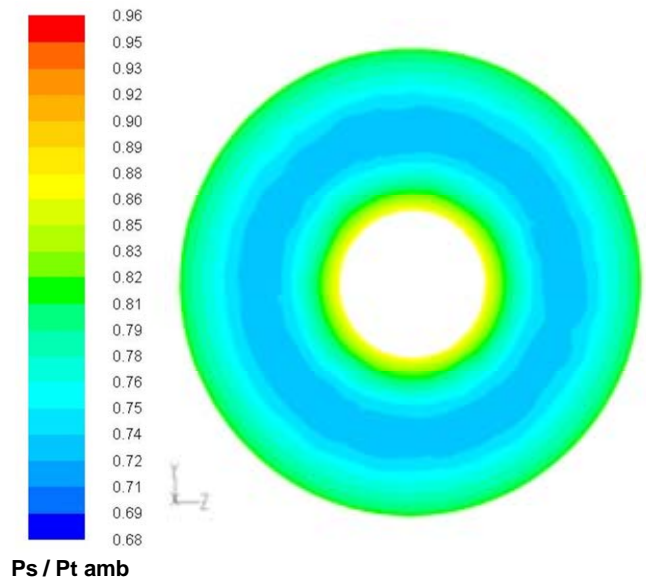


**Figure 1 : Normalized Fan Face Static Pressure Profile (Takeoff Power set) used for the Rotor-less CFD Model Evaluation**

**Description of the Model**

The aircraft surfaces including the fuselage, pylon, wing, nacelle, ground, and far field are modeled for this simulation. These aircraft surfaces represent a typical modern, aft mounted nacelle business jet application in the HTF7000 engine series thrust class. As for all aft mounted nacelles, the engine and nacelle are connected to aft fuselage and it is in close proximity to the fuselage and the wing. The details of the aircraft model and far-field geometry is shown in Figure 2

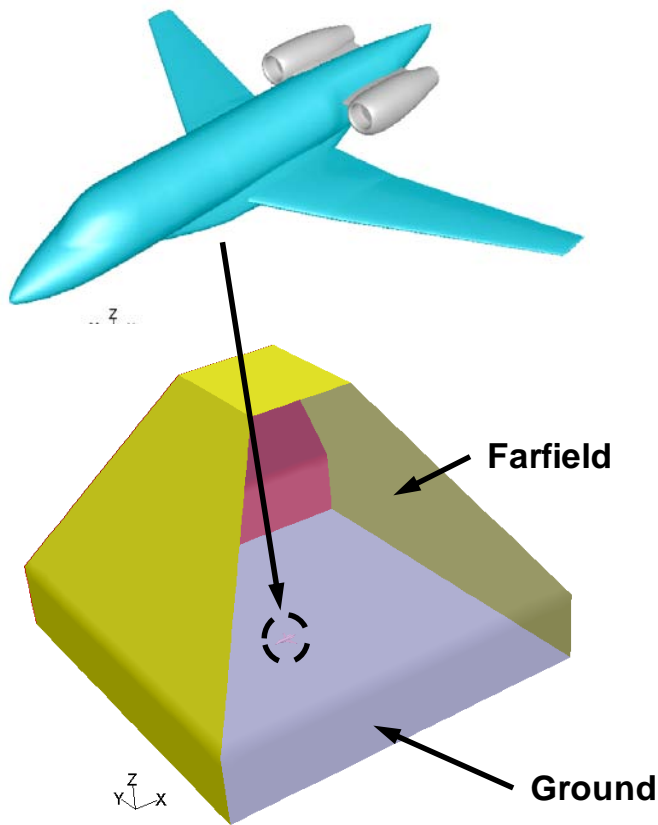


**Figure 2: CFD Model Surfaces**

More modern aircraft designs are better at lowering the impact of fuselage based vortex formation by increasing the gap between the fuselage and the nacelle installation. In the modern aircraft designs more distance is maintained between the nacelle and the fuselage (Figure 3) by incorporating fuselage/nacelle area ruling.

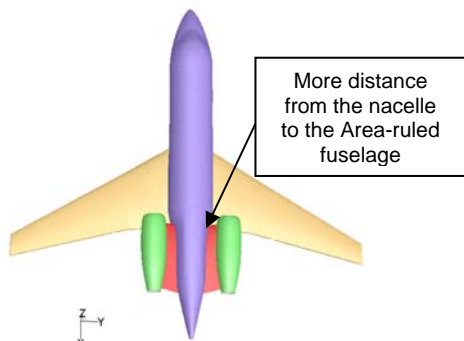


**Figure 3: Aircraft Nacelle and Fuselage**

The HTF7000 fan rotor and stator system was installed into the aircraft nacelle. The intent of adding the fan and stator system within the airframe and inlet model is to aid in properly modeling of flow through the inlet system where separation and attachment can be dictated by the characteristics of the fan immediately downstream of the inlet. The fan/stator system will allow the flow through the inlet to be set by the fan geometry and the fan speed. The meshed rotor and stator geometry and rotating reference frame interfaces are shown Figure 4.

**Fan rotor stator geometry**

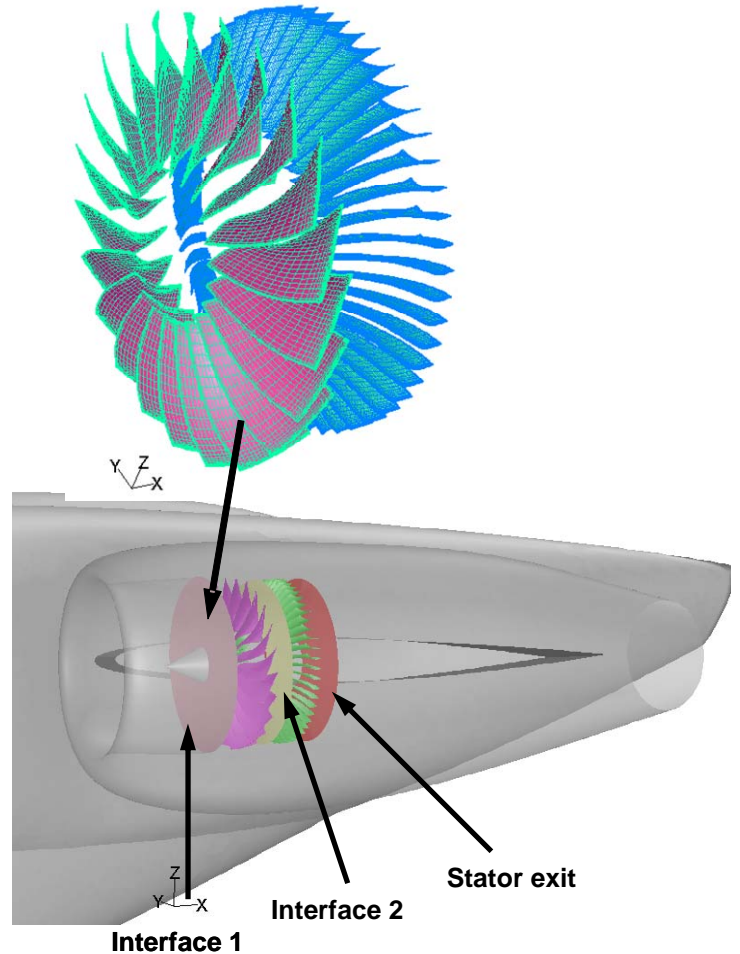


**Figure 4: HTF7000 Fan Rotor and Stator**

Complete modeling of the fan and fan stator installed with the aircraft helps in predicting the 3-D flow characteristics, within the inlet, accurately. CFD analyses were performed at ground idle and take-off operating conditions at different crosswind and headwind velocities. The flow effects external to the aircraft were modeled by creating the far field around the aircraft as shown in Figure 2.

Modeling, trimming and the surface meshing of the aircraft geometry was performed using MSC Patran software. Fan rotor and stator modeling was performed using ANSYS's Autogrid meshing tool. The fan interface location should be modeled accurately in both the models, as the models are combined in Fluent using the interface option.

### **Meshing details**

The CFD mesh was created to include all of the critical aircraft, nacelle, pylon and fan geometries. The volume meshing of the aircraft model was created using ANSYS Tgrid software. Fan rotor and stator geometry was defined as a geom-turbo file and the volume mesh was created using Autogrid. Prisms were grown on the nacelle, fan face and spinner to predict the boundary layer inside the nacelle inlet region. Mesh details are

shown in Figure 4 and Figure 5. Total volume mesh size is greater than 9 million cells for the combined aircraft nacelle and the fan rotor stator. The fan geometry was not meshed in detail since the goal of the analysis was to provide a flow field through the inlet with fan-like characteristics, but not to generate detailed specific fan performance. The final model size was set by the computer memory limitations and scheduling considerations.

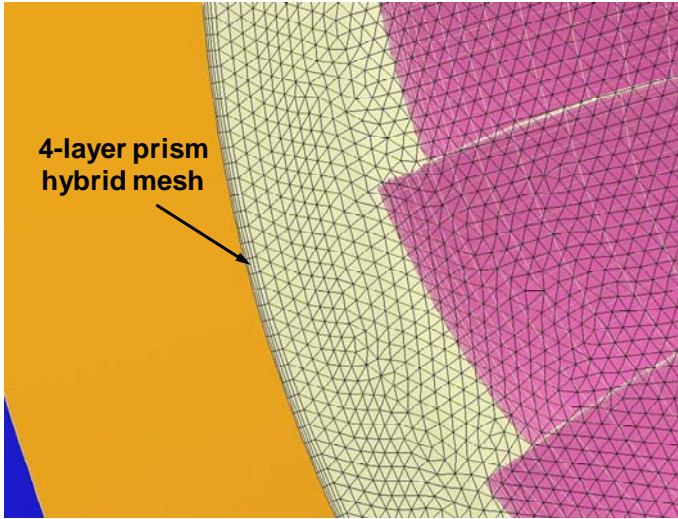


**Figure 5: 4-Layer Hybrid Volume Mesh around the Inlet and Nacelle**

### Boundary Conditions Setup

The CFD analysis performed to predict the distortion effects on the HTF7000 fan was completed using FLUENT's segregated solver. Various crosswind and headwind velocities effects were evaluated at ground idle and takeoff engine operating conditions. Following are the different cases studied for this analysis

- Crosswind
  - 10, 20, 30 Knots (Wind velocities)
  - For all evaluations, the port engine is the upwind engine
- Headwind
  - 10, 20, 30, 50, 75 Knots (Wind velocities)

Takeoff (all conditions)

Fan physical speed = 92% corrected speed → Fan corrected flow set to  $W_c/A_{inlet\ throat} = 0.278 \text{ lbm/s-in}^2$   
 Nozzle physical flow set to inlet flow, Temperature set to engine cycle level.

Ground Idle (for wind velocities 30 Knots or less)

Fan physical speed = 92% corrected speed → Fan corrected flow set to  $W_c/A_{inlet\ throat} = 0.063 \text{ lbm/s-in}^2$   
 Nozzle physical flow set to inlet flow, Temperature set to engine cycle level.

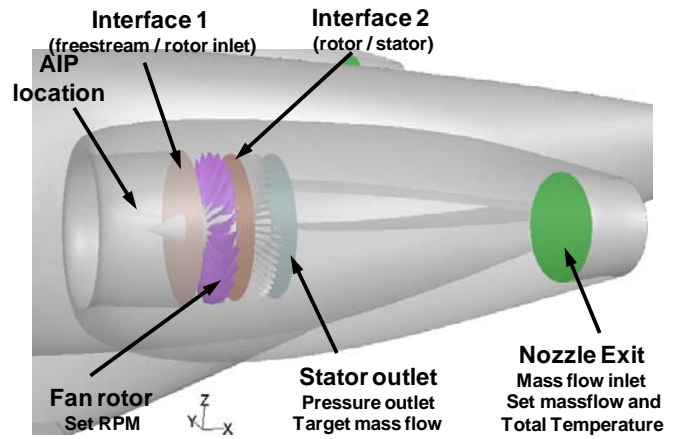


**Figure 6: Boundary Conditions**

FLUENT's SST  $k-\omega$  turbulence model was used for the analysis. Turbulence intensity and turbulence viscosity ratio were specified. The wall  $y^+$  for the inlet wall surfaces were less than 200 for the models representing takeoff power conditions. The highest  $y^+$  values were located on the inlet lip between the inlet highlight and the inlet throat.

The aircraft nacelle Tgrid mesh and the rotor stator mesh from Autogrid were combined in FLUENT using an interface boundary condition (Figure 6). The axis of origin of the rotor stator was defined accurately to avoid any divergence in the solution.

### Results and Discussion

CFD analyses were completed to predict the effects of fuselage and ground based vortices on inlet distortion and the engine fan flow characteristics. Six crosswind velocities and ten headwind velocity cases were studied for this analysis.

#### Headwind results: Ground Idle Condition

CFD analyses were completed for 10, 20, 30 knots headwind cases at the ground idle engine power set condition. It was observed that there is a minimal presence of a vortex on the aircraft fuselage observed for all the headwind velocities at the ground idle condition. No vortices were seen on the aircraft wing. The static pressure isobars shows the vortex formation on the aircraft fuselage are shown in Figure 7

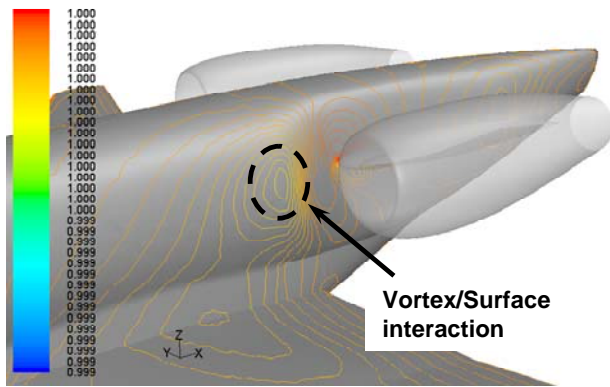


**Figure 7: Normalized Static Pressure (Ps/Pamb) Isobars on the Fuselage: 10 Knot Headwind Case, Ground Idle Condition.**

Minimal vortex effects were apparent on the fan face location for the 10, 20 and 30 knot headwind cases for the ground idle powerset evaluations. Total pressure contours at the AIP location are shown in Figure 8. The effect of fuselage based vortices on the fan flow was observed to be minimal for the headwind cases at the ground idle condition.

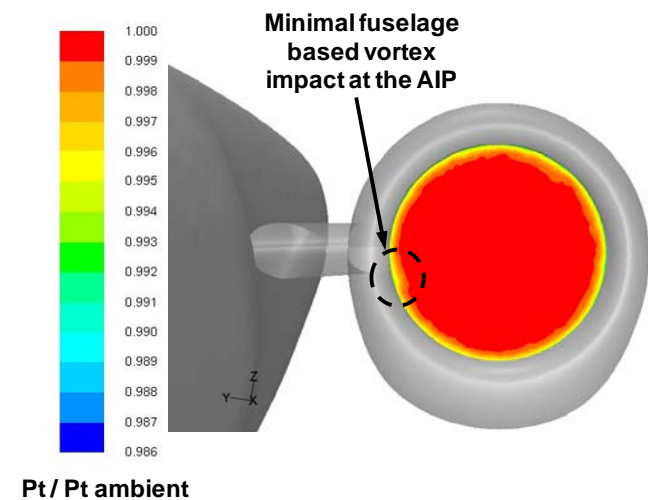


**Figure 8: Normalized Total Pressure Contours at the Fan Face Location – 10 knot Headwind Case, Ground Idle Condition.**

**Headwind Results: Takeoff Condition**

The CFD analyses were completed for 10, 20, 30, 50 and 75 knots headwind cases at the takeoff powerset condition. The presence of a vortex on the aircraft fuselage was observed for all the headwind velocities evaluated at the take-off condition. A vortex is apparent if a circular low static pressure region is seen on the surface of the fuselage.

For the 10 knot headwind velocity case, a vortex is observed on the aircraft fuselage. Static pressure contours on the fuselage

surface and pathlines from the showing the vortex attachment on the fuselage is plotted in Figure 9. Vortices were seen on the aircraft fuselage for 20, 30, 50 and 75 knot headwind cases at the takeoff powerset condition. Static pressure contours on the aircraft fuselage are shown in Figure 10 for the 20 knot and 30 knot headwind cases.

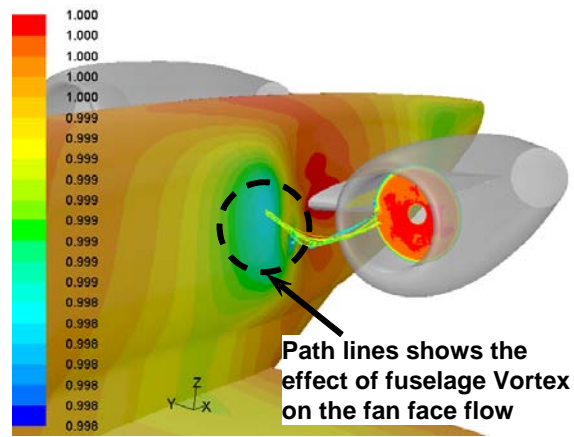


**Figure 9 : Normalized static Pressure (Ps/Pamb) contours on the Fuselage – 10 Knot Headwind Case, Takeoff Condition.**

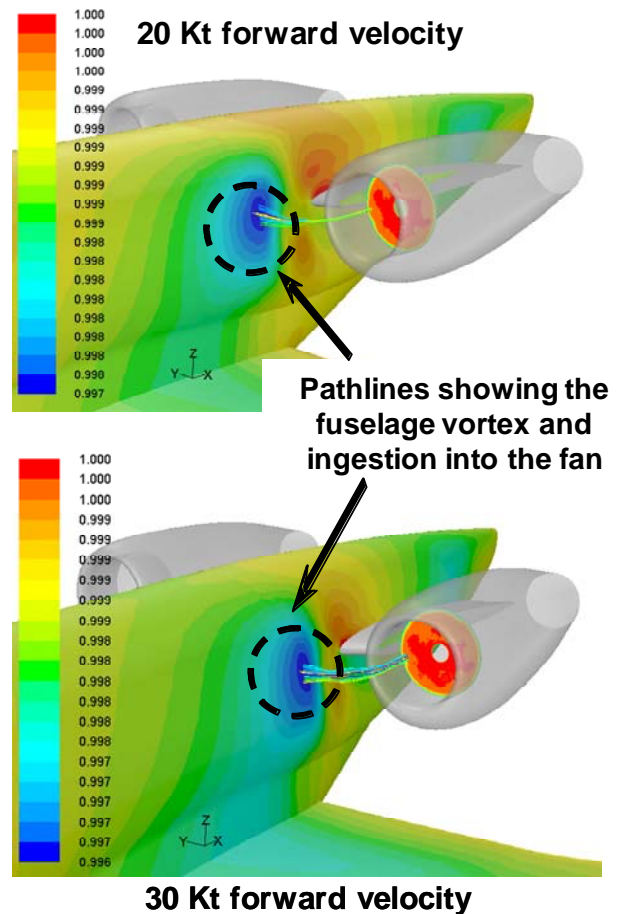


**Figure 10: Normalized Static Pressure (Ps/Pamb) Contours on the Aircraft Fuselage – 20 and 30 knot Headwind Cases, Takeoff Condition.**

Vortex formation from the fuselage was observed affecting the flow at the AIP location for the 10, 20 and 30 knot headwind cases. The total pressure contours at the AIP location for the 10 knot headwind case are plotted in

Figure 11. The low pressure disturbance on the AIP plane shows the effect of the fuselage based vortex.

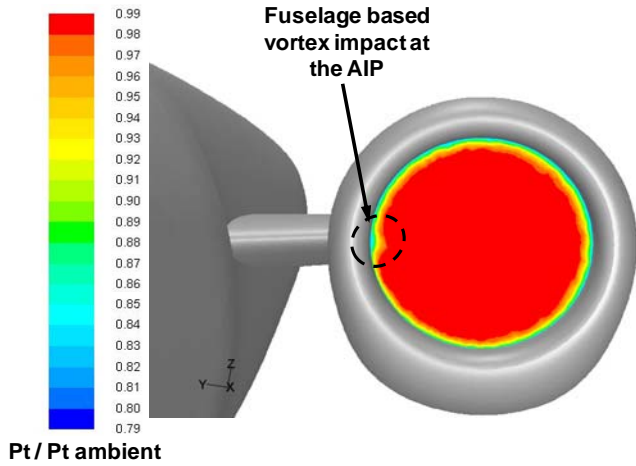


**Figure 11: Normalized Total Pressure Contours at the AIP Location – 10 Knot Headwind Case, Takeoff Condition.**

The vortex effects were observed to be lesser on the flow near the fan face location for the 50 and 75 knots headwind cases. No flow separation was observed for head wind cases at the nacelle inlet. These results are not presented in this paper. For the headwind velocity study, the presence of vortices and their effects are more observed at takeoff powersets compared to ground idle operating powersets.

**Crosswind Results: Ground Idle Condition**

CFD analysis on the HTF7000 series nacelle combined with HTF7000 rotor-stator was completed for 10, 20, 30 knots crosswind cases at ground idle condition. The presence of a vortex on the aircraft fuselage was minimal. However, a circular low pressure region is seen which indicates the presence of a vortex on the downwind engine side fuselage and the aircraft wing. The static pressure contours on the fuselage on both the upwind and downwind sides of the aircraft fuselage are shown in Figure 12

Flow separation was observed for all the cross wind cases at the nacelle inlet. This flow separation will affect the flow conditions at the rotor face. Figure 13 shows the Mach number contours on the plane cutting through the separated region of the fan face location. A recirculation zone is observed at the freestream / fan rotor interface, immediately prior to the flow entering the fan.

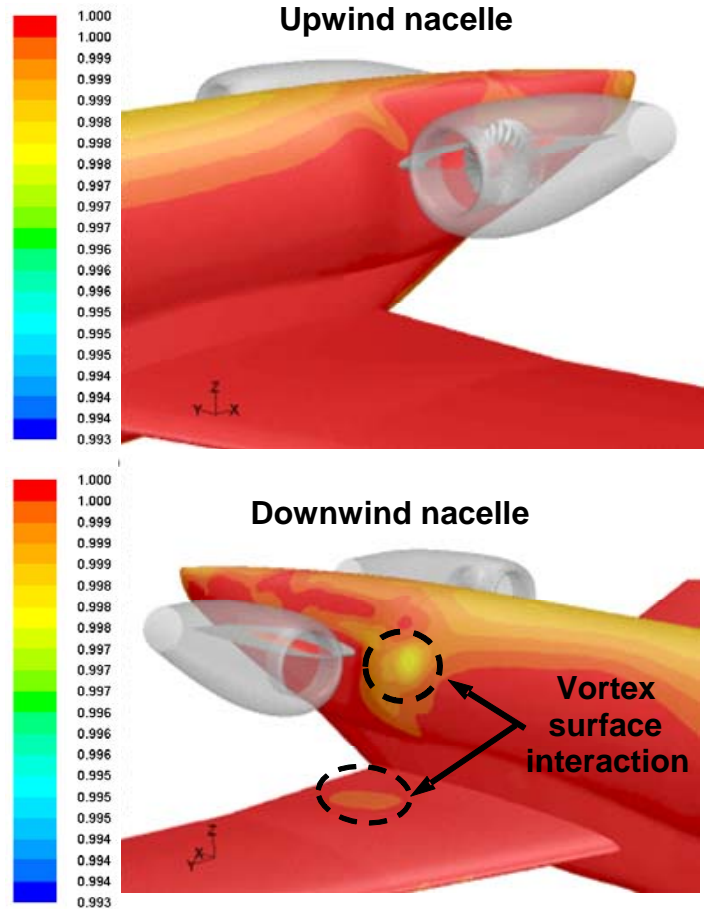


**Figure 12: Normalized Static Pressure ( $P_s/P_{amb}$ ) contours (psi) at the Aircraft Fuselage and Wing – 20 knot Crosswind, Ground Idle Condition.**

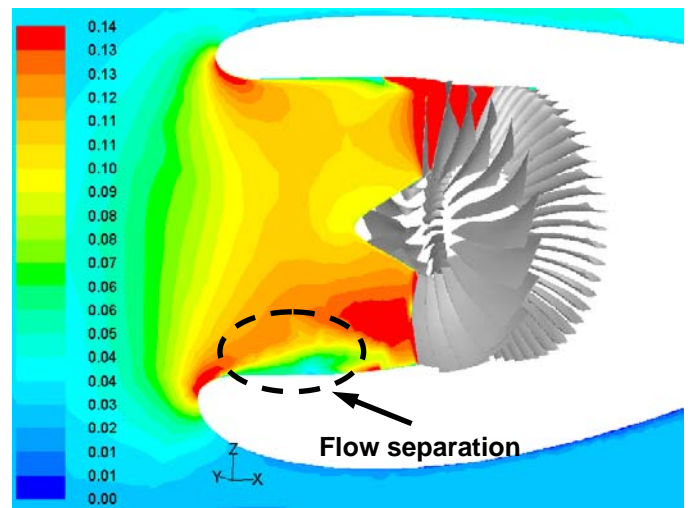


**Figure 13: Mach Number Contours – 20 Knot Crosswind Case, Ground Idle Condition**

The effects of crosswind flow on the fan flow are high, due to high flow separation occurring from the nacelle lip. Total pressure contours are plotted at the AIP showing the effects of flow separation due to crosswind in Figure 14

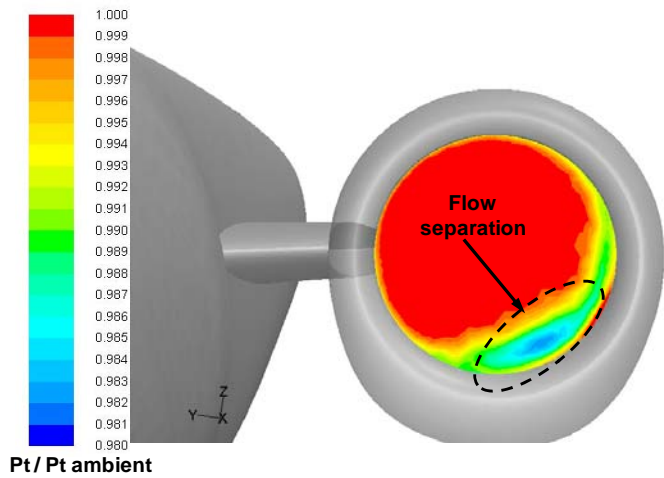


**Figure 14: Normalized Total Pressure at the AIP Location – 20 Knot Crosswind, Ground Idle Condition**

**Crosswind Results: Takeoff Condition**

CFD analysis on the HTF7000 nacelle combined with HTF7000 rotor-stator was completed for 10, 20, 30 knots crosswind cases at take-off condition. The presence of a vortex on the aircraft fuselage was observed mainly for 20 and 30 knot cases. Figure 15 and Figure 16 shows the static pressure contours for the upwind engine for these cases.

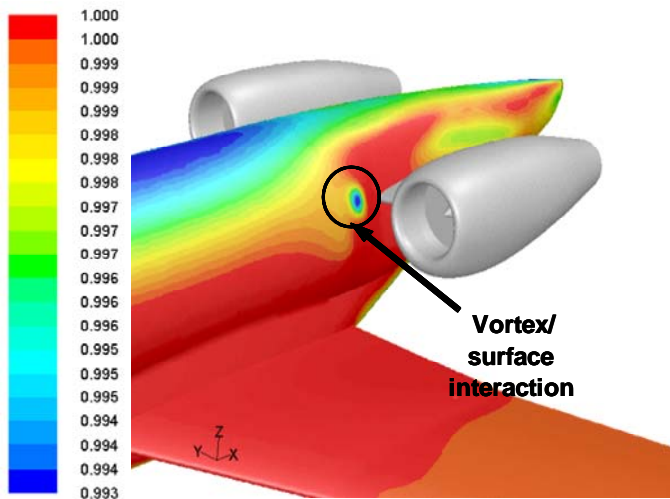


**Figure 15: Normalized Static Pressure (Ps/Pamb) Contours on the Aircraft Fuselage – 30 Knot Crosswind Cases, Takeoff Condition.**

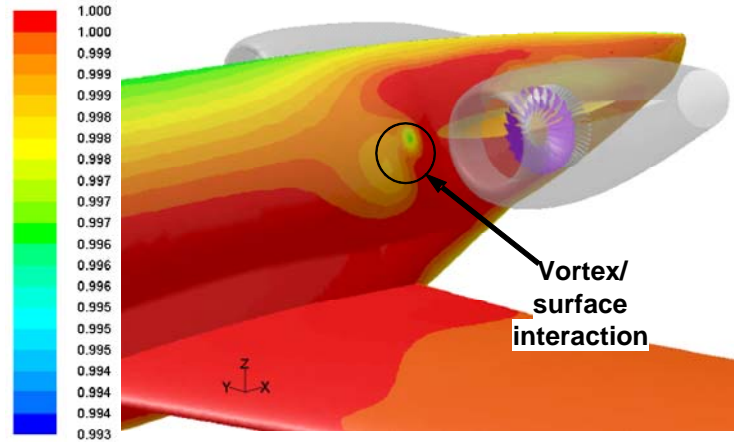


**Figure 16: Normalized Static Pressure (Ps/Pamb) Contours on the Aircraft Fuselage – 20 Knot Crosswind Case, Takeoff Condition.**

Mach number contours (Figure 17) at the fan face show the flow separation near the nacelle inlet. However, the flow separation diminishes before the flow enters the fan. The total pressure contours at the AIP location (Figure 18) shows the effect of flow separation at the AIP location which creates a high distortion region. Additionally, the effects of a fuselage based ground vortex can be seen on the downwind side of the inlet, near the pylon.

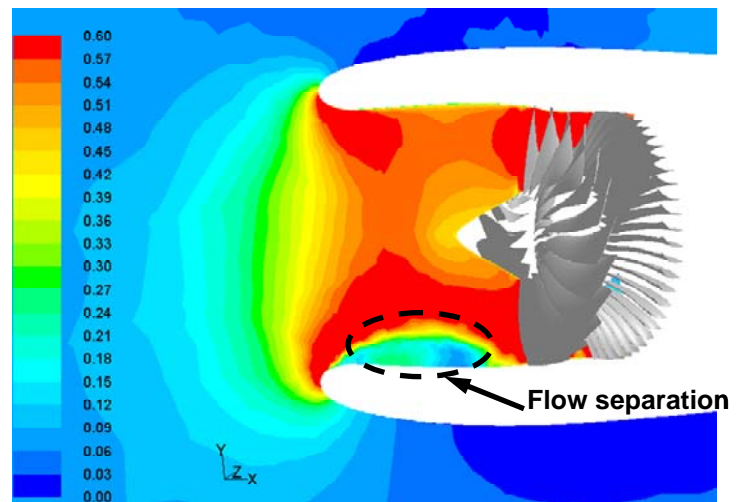


**Figure 17: Mach Number Contours on a Horizontal Plane through the Inlet – 30 Knot Crosswind, Takeoff Condition.**

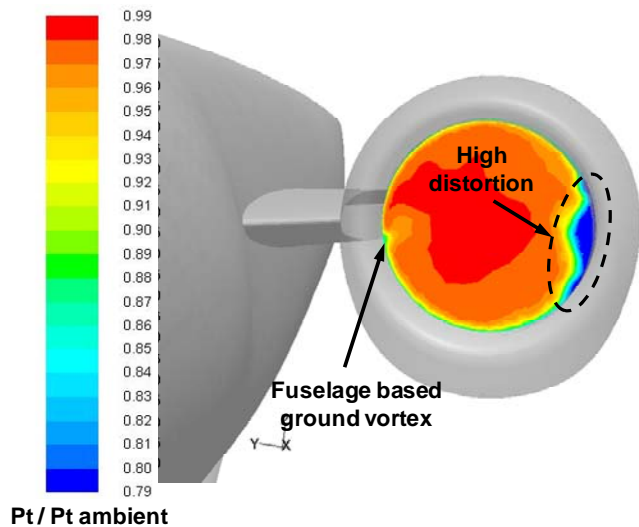


**Figure 18: Normalized Total Pressure Contours at the AIP location – 30 knots Crosswind case, Take-off Condition**

Overall, the crosswind study shows the formation of fuselage based vortices for all wind velocities at ground idle and takeoff conditions. The analyses also show significant flow separation on the upwind side of the inlet inner barrel which will cause high levels of circumferential distortion.

**Distortion Parameter Description**

A figure of merit on the relative accuracy for CFD analyses relative to test data is the comparison of calculated circumferential and radial distortion parameters. Circumferential and radial distortion is discussed in SAE ARP 1419. These distortion parameters, as well as parameters for mechanical distortion are typically measured for engine/nacelle configurations during the Part 25 certification process for aircraft development.

Inlet distortion is measured at the inlet aerodynamic interface plane (AIP) using a series of fixed total pressure rakes. For the HTF7000 series of nacelles, 10 circumferentially equally spaced rakes with 6 probe immersions are located at centers of equal areas. For the HTF7000 series of nacelles, the AIP is located in the inlet, 5.10 inches forward of the engine/inlet connect flange. The schematic for the inlet distortion rakes, and a photograph of the inlet distortion rakes installed in the HTF7000 inlet is shown in Figure 19.

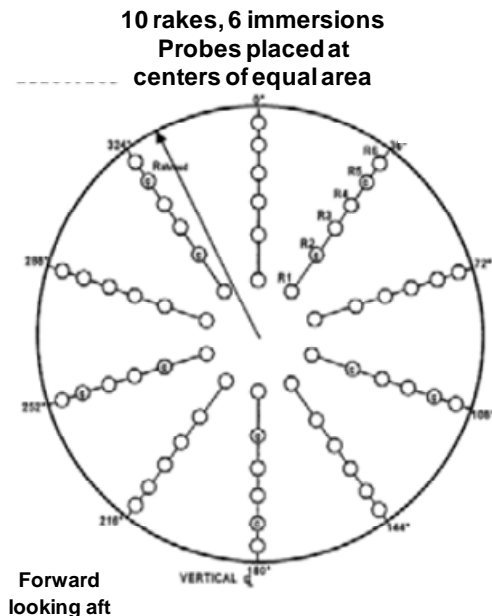


**Figure 19 : HTF7000 Inlet Distortion Rake Schematic and 10 Rake, 6 Immersion Installation in a HTF7000 Inlet.**

**Distortion Evaluation and Comparison**

Total pressures were extracted from the various crosswind and headwind FLUENT CFD runs. The extracted pressure data was for a base of six immersions at centers of equal areas, similar to the HTF7000 nacelle test inlet; however data was extracted for an equivalent of 10, 60 and 180 rakes in order to increase the information density for the circumferential and radial distortion evaluations. The pressure information was evaluated for circumferential and radial distortion using the processes set forth in SAE ARP 1419. Specifically, circumferential distortion is defined as the maximum ring value for intensity where intensity is based on average pressures and is defined as:

$$(\Delta P_C/P)_i = (PAV_i - PAV_{LOW_i}) / PAV_i$$

Radial distortion is defined as the maximum ring value for intensity radially where intensity is based on average pressures and is defined by:

$$(\Delta P_R/P)_i = (P_{FAV_i} - P_{AV_i}) / P_{FAV_i}$$

Results for crosswind distortion, using the rotating reference frame frozen rotor model, for the upwind engine at takeoff power for various rake densities are shown in Figure 20. This figure additionally shows a region which is representative of distortion test data for the HTF7000 series of nacelles. Also plotted is the 10 rake, 6 immersion data at the AIP location for a rotor-less analysis using a static profile at the fan face location. The results show the CFD predicted circumferential distortion is significantly greater than the test data. The results also show for circumferential distortion, the number of rakes is not critical in prediction of circumferential distortion levels. The analysis shows the rotor-less model, using the static pressure profile at the fan face (AS907-1 CFD data), has the same level of results as the full fan/stator rotating reference frame model.

Figure 21 shows the equivalent evaluation for radial distortion (90° crosswind, upwind engine, takeoff power). Results show the CFD significantly over-predict tested results. The results show minimal variation for increasing rake density. The results show the rotor-less model, using the static pressure profile at the fan face (AS907-1 CFD data), has a slightly lower level of radial distortion than the full fan/stator rotating reference frame model.

Figure 22 shows circumferential distortion results for headwind conditions, using the rotating reference frame frozen rotor model, for the upwind engine at takeoff power for various rake densities. The CFD results are compared to measured test data. The results show good correlation to test data, although the CFD predictions are greater than the measured test data.

Figure 23 shows radial distortion results for headwind conditions, using the rotating reference frame frozen rotor model, for the upwind engine at takeoff power for various rake densities. The CFD results are compared to measured test data. The CFD results are significantly greater than the test data. The higher level of radial distortion is likely due to an insufficiently high prism boundary layer mesh on the inlet surfaces. The insufficiently high boundary layer mesh allowed pressure diffusion into the inlet diffuser flow stream which affected the outer ring total pressure levels. Artificially lower total pressure levels on the outer ring would produce higher levels of radial distortion.

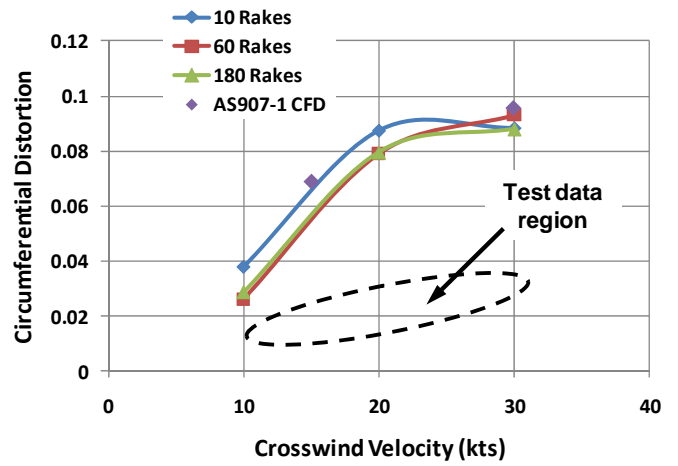


Figure 20: Comparison of Circumferential Distortion for the HTF7000 Series of Nacelles (Upwind engine, Takeoff Power) as a Function of Crosswind Velocity and Rake Density in the CFD Model.

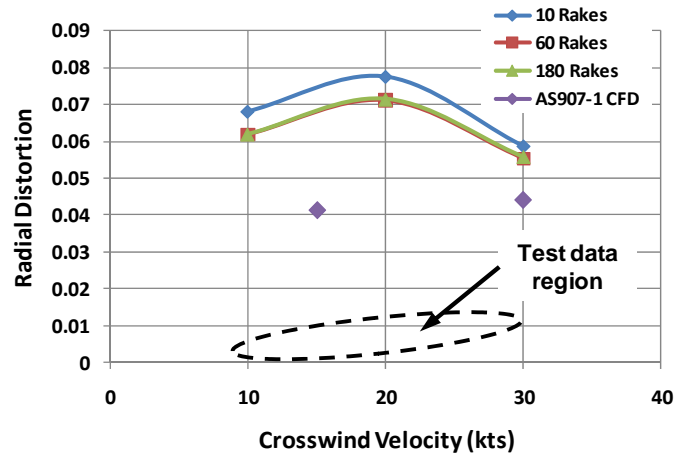


Figure 21: Comparison of Radial Distortion for the HTF7000 Series of Nacelles (Upwind engine, Takeoff Power) as a Function of Crosswind Velocity and Rake Density in the CFD Model.

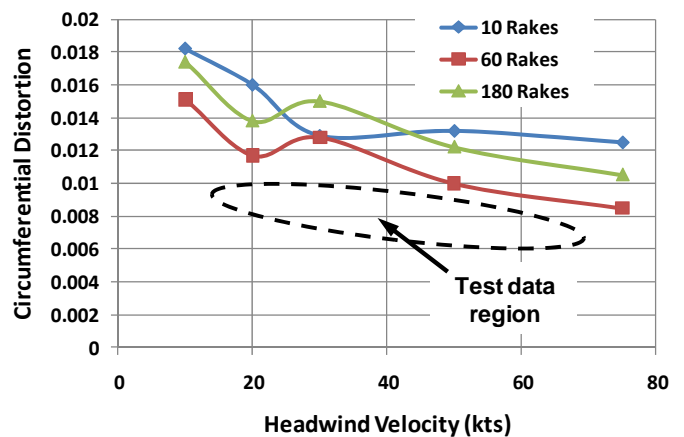
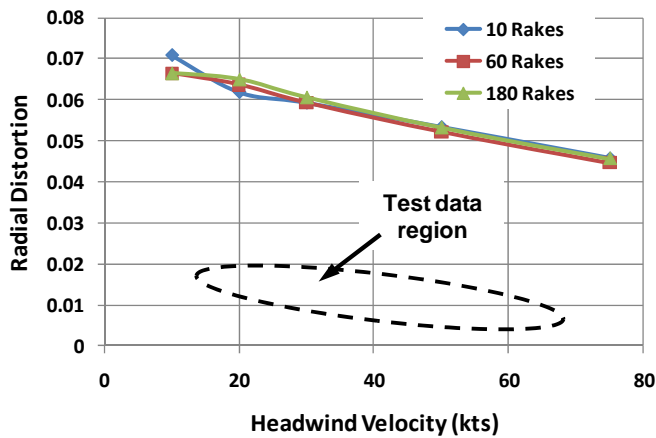


Figure 22: Comparison of Circumferential Distortion for the HTF7000 Series of Nacelles (Port Engine, Takeoff Power) as a Function of Headwind Velocity and Rake Density in the CFD Model.



**Figure 23: Comparison of Radial Distortion for the HTF7000 Series of Nacelles (Port Engine, Takeoff Power) as a Function of Headwind Velocity and Rake Density in the CFD Model.**

### Conclusions

This paper discusses a CFD study to predict pressure distortion on aft fuselage mounted turbofan inlets for various crosswind and headwind conditions where fuselage based vortex effects can be seen. CFD was performed using a frozen rotor in a rotating reference frame. The analysis was done at ground idle and takeoff engine powerset conditions.

For the headwind velocity study, the presence of vortices and their effects are more severe at take-off conditions when as opposed to the ground idle powerset condition. The fuselage based vortex appears to have a minor effect on fan flow and distortion. If measured by a stationary distortion rake during flight test, the effect may appear as an intermittent pressure anomaly on one of the distortion rakes.

During crosswind conditions, the presence of a fuselage based vortex was observed mainly for 20 and 30 knot crosswind cases. Velocity vectors at the fan face location had shown the flow separation near the nacelle inlet, though the flow separation diminishes before the flow enters the fan.

A comparison of circumferential and radial pressure distortion was performed for the HTF7000 nacelle at the AIP location:

- CFD model using a frozen rotor, rotating reference frame,
- CFD model using a static pressure profile at the fan face location
- Test data

The distortion evaluation used SAE ARP 1419 descriptors for

circumferential and radial distortion. The comparison shows the CFD models over-predict distortion levels relative to test data. The over-prediction in circumferential and radial distortion is believed to be due to insufficient boundary layer mesh definition in the inlet inner barrel and mesh element coarseness at the inlet lip. Insufficient mesh size occurred from limitations on computer memory and time constraints at the timeframe of the analysis. Insufficient boundary layer definition will allow excessive boundary layer growth in the diffusing inlet inner barrel.

This paper highlights the inlet distortion modeling capability of CFD for crosswind and forward operation conditions which include the effects of fuselage and ground based vortices on the aircraft nacelle which is installed with fan rotor and stator geometry.

### References

1. SAE Aerospace Information Report AIR-1419, "Inlet Total-Pressure Distortion Considerations for Gas Turbine Engines," May 1983.
2. Rodert, L. A. & Garrett, F. B., "Ingestion of Foreign Objects into Turbine Engines by Vortices," National Advisory Committee for Aeronautics, NACA TN 3330, 1953.
3. Glenn, D. E. and Pyestock, N. G. T. E., "Ingestion of Debris into Intakes by Vortex Action," C.P. No. 1114, 1968.
4. Motycka, D.L., "Ground Vortex - Limit to Engine/Reverser Operation," Transactions of the ASME Gas Turbine Conference, Vol. Paper No. 75- GT-3, Transactions of the ASME, 1975.
5. Shin, H. W., Greitzer, E. M., Cheng, W. K., Tan, C. S. and Shippee, C. L., "Circulation Measurements and Vortical Structure in an Inlet Vortex Flow Field," Journal of Fluid Mechanics, Vol. 162, 1986, pp. 463-487.
6. Shin, H. W., Cheng, W. K., Greitzer, E. M. & Tan, C. S., "Inlet Vortex Formation due to Ambient Vorticity Intensification," American Institute of Aeronautics and Astronautics, Vol. 24, No. 4, 1986, pp. 687-689.
7. Murphy, J. P. and MacManus, D. G., A Quantitative Study on Inlet Ground Vortices, AIAA-ISABE-207-1209.
8. SAE Aerospace Information Report AIR5686, "A Methodology for Assessing Inlet Swirl Distortion", July 25, 2009.